International Journal of Solids and Structures 46 (2009) 2999–3008

Contents lists available at ScienceDirect

International Journal of Solids and Structures

journal homepage: www.elsevier.com/locate/ijsolstr

A new boundary element approach of modeling singular stress fields of plane V-notch problems

Zhongrong Niu [a,*], Changzheng Cheng [a,c], Jianqiao Ye [a,b], Naman Recho [c]

[a] School of Civil Engineering, Hefei University of Technology, Hefei 230009, PR China
[b] School of Civil Engineering, The University of Leeds, Leeds LS2 9JT, UK
[c] ERMESS/EPF-Ecoles d'Ingénieurs, Sceaux and LaMI/Univ.B.Pascal, Clermont Fd., France

ARTICLE INFO

Article history:
Received 13 October 2008
Received in revised form 30 March 2009
Available online 7 April 2009

Keywords:
Linear elasticity
V-notch
Stress intensity factor
Boundary element method
Asymptotic expansion

ABSTRACT

In this paper, a new boundary element (BE) approach is proposed to determine the singular stress field in plane V-notch structures. The method is based on an asymptotic expansion of the stresses in a small region around a notch tip and application of the conventional BE in the remaining region of the structure. The evaluation of stress singularities at a notch tip is transformed into an eigenvalue problem of ordinary differential equations that is solved by the interpolating matrix method in order to obtain singularity orders (degrees) and associated eigen-functions of the V-notch. The combination of the eigen-analysis for the small region and the conventional BE analysis for the remaining part of the structure results in both the singular stress field near the notch tip and the notch stress intensity factors (SIFs).

Examples are given for V-notch plates made of isotropic materials. Comparisons and parametric studies on stresses and notch SIFs are carried out for various V-notch plates. The studies show that the new approach is accurate and effective in simulating singular stress fields in V-notch/crack structures.

1. Introduction

V-notches of bonded dissimilar materials are frequently encountered in engineering applications, such as in welded connections and structures strengthened with fiber reinforce polymer plates. In such cases, the stress concentration near the sharp notch and the interface end is very high. In particular, the peak stress at the notch tip is singular according to the theory of elasticity. For evaluating fatigue strength of the structures, the stress distribution around the notch tip and the notch/generalized stress intensity factors (GSIFs) are important mechanical quantities to be determined. Since there exist multiple stress singularities at a general V-notch structure, it is difficult to model the singular stress field by conventional methods. Analytical solutions of the notch SIFs have been found only for a few special cases.

Extensive studies have been carried out to deal with the singular stress fields of V-notch problems. Gross et al. (1964), Gross and Mendelson (1972) and Carpenter (1984) obtained the GSIFs for plane V-notch problems by a boundary collocation method. Chen (1995) derived the notch SIFs of some plane V-notch problems by using the body force method, in which the density functions associated to the body forces had to be configured in advance. By applying Lekhnitskii formalism and Stroh formalism, Ting (1996) studied the solutions of the stress fields of general anisotropic elastic materials and composites. For the two-dimensional V-notches, Szabó and Yosibash (1996) obtain first a conventional finite element method solution for the entire domain, which was then used as boundary conditions of a small sub-domain around the notch tip. Then a special finite element formulation in conjunction with the assumption of the asymptotic expansion of the displacement field in the sub-domain, where the singular eigen-pairs have been obtained by other methods, is used to extract the GSIFs. Evidently, the efficiency of the method depends on the accuracy of the preliminary FE solution. Matsumoto et al. (2000) derived a boundary integral expression of the interaction energy release rate for a cracked body and computed the stress intensity factors of bimaterial interfacial cracks. Based on the analytical expressions of the local stress field near a V-notch tip, Atzori et al. (2002) estimated the fatigue strength of welded joints with notches in aluminum alloys at a given number of cyclic loading. With the solutions of stress singularities, Labossiere and Dunn (1999) and Hwu and Kuo (2007) computed the stress intensity factors through the near tip displacement and stress fields from the conventional finite element analysis as well as the calculation of the path-independent *H*-integral (Stern et al., 1976). Based on a critical interface corner stress intensity factor, Reedy and Guess (1993) gave a failure criterion for the strength of the adhesively bonded butt tensile joint. Gómez and Elices (2003) presented a simple approximate formulation of fracture criterion for sharp V-notches of some materials, such as steel, aluminum PMMA and PVC. Utilizing the results of the GSIFs, Livieri and Lazzarin (2005) evaluated the fatigue strength of steel and

* Corresponding author. Tel.: +86 551 2901437; fax: +86 551 2902066.
E-mail address: niu-zr@hfut.edu.cn (Z. Niu).

0020-7683/$ - see front matter © 2009 Elsevier Ltd. All rights reserved.
doi:10.1016/j.ijsolstr.2009.03.028

aluminum welded joints as a type of V-notched structures by studying on a large amount of experimental data. By using coherent gradient sensing (CGS) method, Yao et al. (2006) experimentally studied mode-I stress singularity and fracture behaviors of V-notch tip.

At present, the most commonly used numerical methods to determine stress distributions of a V-notch are the finite element and boundary element methods (BEM). The conventional FEM (Pageau et al., 1995; Mohammed and Liechti, 2001) and BEM (Tan et al., 1992; Xu et al., 1999; Ioka et al., 2007) usually use very fine meshes in the vicinity of the notch tip to simulate the singular stress field. Then the stresses or displacements at some mesh points near the notch tip are used to determine the GSIFs by the extrapolation technique. However, any further increase of element number has very limited impact on improving the accuracy of the approaches. This is because the conventional elements near the notch tip cannot reflect the essence of the stress singularity in the tip region. It is well known in the finite element analysis that the "quarter-point" element (Henshel and Shaw, 1976; Barsoum, 1976) at crack tip can efficiently model the singular stress field near the crack tip, in which the mid-side nodes near the crack tip are placed at the quarter point. Subsequently the idea was introduced to the BEM by Blandford et al. (1981). In fact, the shape functions of the quarter-point element can only represent stress singularity of order $-1/2$ that is correct for line cracks of isotropic materials. Unfortunately the quarter-point element is not suitable to model the stress field near a V-notch tip. Researchers have been trying for some time to construct a singular element for modeling stress fields in the notch tip region. To the authors' best knowledge, it has not been very successful.

On the basis of asymptotic expansion of the stresses near a V-notch tip, a special finite element method was recently used to deal with some V-notch problems. For V-notches and line cracks, according to the singular stress fields of the type $\sigma_{ij} = r^{\lambda} f_{ij}(\theta)$, Seweryn (2002) took two or three dominating stress eigen-functions as analytical constrains in the notch tip region. Then the resulting elements in terms of the analytical constrains were applied to model the stress field in the core region around the notch tip. The remaining area of the notched structure can be modeled using the conventional FEM. This approach requires predefined analytical stress eigen-functions. For the V-notch of isotropic materials subjected to various boundary conditions, Seweryn and Molski (1996) gave the analytical solutions of the eigen-functions, and explicit closed-form eigen equation, from which the eigenvalues can be determined by an iteration technique. However the analytical stress eigen-functions are not always acquirable for general V-notch problems of bonded dissimilar multi-material. To address this problem, some approximate stress eigen-functions were proposed to construct the stress functions. For example, using the FEM, Carpinteri et al. (2006) calculated the first leading singular exponent and the mode I stress amplitude for a multi-layered beam with a crack or re-entrant corner that forms symmetrically a bimaterial interface. Chen and Sze (2001) proposed a hybrid finite element with asymptotic expansion to determine the stress exponents and stress distributions of bonded bimaterial V-notches. On the basis of this work, Sze et al. (2001) and Chen and Ping (2007) developed the approach further and used it for the analyses of singular electro-elastic fields around a V-notch of piezoelectric material. By the same method, Ping et al. (2008) analyzed the singular stress fields of V-notched anisotropic plates.

In this study, a new BE approach is proposed to determine the singular stress fields of plane V-notch structures in conjunction with asymptotic expansions of the stress distribution near the notch tips. To find the stress field near a tip, a small sector around the notch tip is isolated from the V-notch structure as a free body. Based on the expression of the asymptotic expansion, the evaluation of stress singularities in the notch tip region is transformed into an eigenvalue problem of ordinary differential equations (ODEs). The eigenvalue problem is then solved by the interpolating matrix method (Niu, 1993) to obtain the singularity orders and the associated eigenvectors of the V-notch. Further to the eigen-analysis of the small sector, the boundary integral equation is applied to treat the remaining region of the notched structure. Thus the displacement and stress fields of the V-notch structure and the notch SIFs are finally determined.

2. The eigen-analysis of the stress singularities of the plane V-notch problems

Let us consider a plane V-notch of isotropic material with an opening angle $\alpha = 2\pi - \theta_1 - \theta_2$ as shown in Fig. 1. Define a polar coordinate system, $\rho - \theta$, with an origin at the notch tip. Two radial edges of the notch are denoted by Γ_1'' and Γ_2''.

A small sectorial region Ω_R within the range of a radius R of the V-notch tip is cut out from the solid region Ω of the V-notch structure as shown in Fig. 2(b). The remaining part of the notch structure is referred to as region Ω' (see Fig. 2(a)). There are $\Omega = \Omega' \cup \Omega_R,\ \Gamma_i'' = \Gamma_i \cup \Gamma_i',\quad (i = 1, 2)$.

In the linear elasticity, it has been verified that the asymptotic displacement field in the notch tip region can be expressed as a series expansion with respect to the radial coordinate ρ originating from the notch tip (Yosibash and Szabó, 1996). A typical term of the series can be written in the form

$$\begin{cases} u_{\rho k}(\rho,\theta) = A_k \rho^{\lambda_k+1} \tilde{u}_{\rho k}(\theta) \\ u_{\theta k}(\rho,\theta) = A_k \rho^{\lambda_k+1} \tilde{u}_{\theta k}(\theta) \end{cases} \tag{1}$$

where the exponent λ_k is called stress singularity order; $\tilde{u}_{\rho k}(\theta)$ and $\tilde{u}_{\theta k}(\theta)$ are the associated eigen-functions which represent the displacement components in the ρ- and θ-directions, respectively; A_k is the amplitude coefficient of each term of the asymptotic expansion (called also the generalized/notch stress intensity factor). Substituting Eq. (1) into the strain–displacement relations of the linearly elastic theory yields the strain components. Then from Hooke's law of plane stress problems, the components of the plane stress tensor are expressed as

$$\begin{cases} \sigma_{\rho k}(\rho,\theta) = \frac{E}{1-\nu^2} A_k \rho^{\lambda_k} \left[(1+\lambda_k)\tilde{u}_{\rho k} + \nu \tilde{u}_{\rho k} + \nu \tilde{u}'_{\theta k}\right] \\ \sigma_{\theta k}(\rho,\theta) = \frac{E}{1-\nu^2} A_k \rho^{\lambda_k} \left[(1+\lambda_k)\nu\ \tilde{u}_{\rho k} + \tilde{u}_{\rho k} + \tilde{u}'_{\theta k}\right] \\ \sigma_{\rho\theta k}(\rho,\theta) = \frac{E}{2(1+\nu)} A_k \rho^{\lambda_k} (\lambda_k \tilde{u}_{\theta k} + \tilde{u}'_{\rho k}) \end{cases} \tag{2}$$

where $(\cdots)' = d(\cdots)/d\theta$; E is the Young's modulus and ν the Poisson's ratio. If the stress eigen-functions $\tilde{\sigma}_{\rho k}(\theta)$, $\tilde{\sigma}_{\theta k}(\theta)$ and $\tilde{\sigma}_{\rho\theta k}(\theta)$ are defined as follows:

$$\begin{cases} \tilde{\sigma}_{\rho k}(\theta) = \frac{E}{1-\nu^2} \left[(1+\lambda_k)\tilde{u}_{\rho k} + \nu \tilde{u}_{\rho k} + \nu \tilde{u}'_{\theta k}\right] \\ \tilde{\sigma}_{\theta k}(\theta) = \frac{E}{1-\nu^2} \left[(1+\lambda_k)\nu\ \tilde{u}_{\rho k} + \tilde{u}_{\rho k} + \tilde{u}'_{\theta k}\right] \\ \tilde{\sigma}_{\rho\theta k}(\theta) = \frac{E}{2(1+\nu)} (\lambda_k \tilde{u}_{\theta k} + \tilde{u}'_{\rho k}) \end{cases} \tag{3}$$

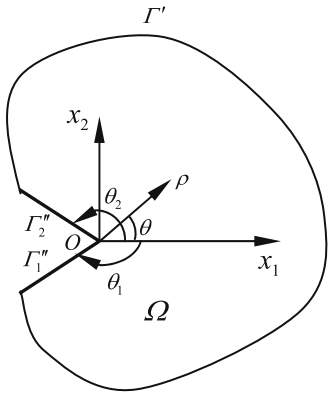

Fig. 1. A plane V-notch problem.

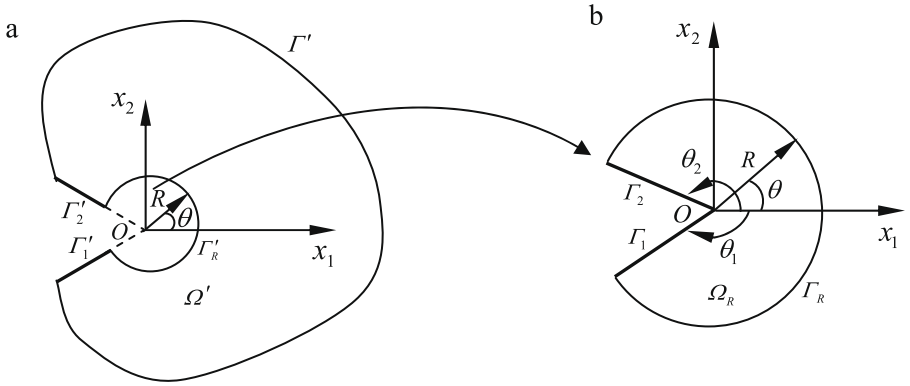

Fig. 2. A plane V-notch. (a) The remaining part after a sector around the notch tip being removed. (b) The sector taken around the notch tip.

The three plane stresses are

$$\begin{cases} \sigma_{\rho k}(\rho,\theta) = A_k \rho^{\lambda_k} \tilde{\sigma}_{pk}(\theta) \\ \sigma_{\theta k}(\rho,\theta) = A_k \rho^{\lambda_k} \tilde{\sigma}_{\theta k}(\theta) \\ \sigma_{\rho\theta k}(\rho,\theta) = A_k \rho^{\lambda_k} \tilde{\sigma}_{p\theta k}(\theta) \end{cases}$$

Note that the eigen-pairs in Eq. (1) do not depend on load conditions. In the small sectorial region Ω_R, the body forces can be neglected and the equilibrium equations are

$$\begin{cases} \frac{\partial \sigma_\rho}{\partial \rho} + \frac{1}{\rho}\frac{\partial \sigma_{\rho\theta}}{\partial \theta} + \frac{\sigma_\rho - \sigma_\theta}{\rho} = 0 \\ \frac{1}{\rho}\frac{\partial \sigma_\theta}{\partial \theta} + \frac{\partial \sigma_{\rho\theta}}{\partial \rho} + \frac{2\sigma_{\rho\theta}}{\rho} = 0 \end{cases} \tag{4}$$

Introducing Eq. (2) into Eq. (4) and removing the common factor $A_k \rho^{\lambda_k - 1}$ from the equations lead to a set of ordinary differential equations (ODEs) as follows:

$$\begin{cases} \tilde{u}''_{\rho k} + \left(\frac{1+\nu}{1-\nu}\lambda_k - 2\right)\tilde{u}'_{\theta k} + \frac{2}{1-\nu}\lambda_k(\lambda_k+2)\tilde{u}_{\rho k} = 0 \\ \tilde{u}''_{\theta k} + \left[2 + \frac{1}{2}(1+\nu)\lambda_k\right]\tilde{u}'_{\rho k} + \frac{1}{2}(1-\nu)\lambda_k(\lambda_k+2)\tilde{u}_{\theta k} = 0 \end{cases}, \quad \theta \in (\theta_1, \theta_2) \tag{5}$$

The appearance of λ_k^2 in Eq. (5) results in a nonlinear eigen problem that is difficult to solve. Here an alternative approach is adopted to transfer the equations into a linear eigenvalue problem. To this end, two new field variables are introduced as below:

$$\begin{cases} g_{\rho k}(\theta) = \lambda_k \tilde{u}_{\rho k}(\theta) \\ g_{\theta k}(\theta) = \lambda_k\ \tilde{u}_{\theta k}(\theta) \end{cases} \quad \theta \in (\theta_1, \theta_2) \tag{6}$$

Hence, by introducing $g_{\rho k}(\theta)$ and $g_{\theta k}(\theta)$ into Eq. (5), one has

$$\begin{cases} \tilde{u}''_{\rho k} + \left(\frac{1+\nu}{1-\nu}\lambda_k - 2\right)\tilde{u}'_{\theta k} + \frac{2}{1-\nu}(\lambda_k+2)g_{\rho k} = 0 \\ \tilde{u}''_{\theta k} + \left[2 + \frac{1}{2}(1+\nu)\lambda_k\right]\tilde{u}'_{\rho k} + \frac{1}{2}(1-\nu)(\lambda_k+2)g_{\theta k} = 0 \end{cases} \quad \theta \in (\theta_1,\ \theta_2) \tag{7}$$

Assume that all the tractions on the two edges, Γ_1 and Γ_2, near the notch tip are zero. That is

$$\left\{ \begin{matrix} \sigma_\theta \\ \sigma_{\rho\theta} \end{matrix} \right\}_{\theta=\theta_1} = \left\{ \begin{matrix} \sigma_\theta \\ \sigma_{\rho\theta} \end{matrix} \right\}_{\theta=\theta_2} = \left\{ \begin{matrix} 0 \\ 0 \end{matrix} \right\} \tag{8}$$

Substitution of Eq. (2) into Eq. (8) yields the boundary conditions as follows:

$$\begin{cases} \tilde{u}'_{\theta k} + (1 + \nu + \nu\lambda_k)\tilde{u}_{\rho k} = 0 \\ \tilde{u}'_{\rho k} + \lambda_k \tilde{u}_{\theta k} = 0 \end{cases} \quad \theta = \theta_1 \text{ and } \theta_2 \tag{9}$$

If the edges are fixed along either Γ_1 or Γ_2, the boundary condition can easily be expressed as

$$\tilde{u}_\rho = 0, \quad \theta = \theta_1 \text{ or } \theta_2 \tag{10a}$$

$$\tilde{u}_\theta = 0, \quad \theta = \theta_1 \text{ or } \theta_2 \tag{10b}$$

By the above derivation, the evaluation of the singularity orders and the associated eigen-functions $\tilde{u}_\rho$ and $\tilde{u}_\theta$ near the V-notch tip is transformed to the solution of a linear eigenvalue problem of the ODEs governed by Eqs. (6) and (7) subjected to the boundary conditions of Eqs. (9) or (10). Through Eq. (3), $\tilde{u}_\rho$ and $\tilde{u}_\theta$ can be used to determine the stress eigen-functions $\tilde{\sigma}_{\rho k}(\theta), \tilde{\sigma}_{\theta k}(\theta)$ and $\tilde{\sigma}_{\rho\theta k}(\theta)$ in the vicinity of the notch tip.

Furthermore, for the analysis of plane V-notch problems of bonded dissimilar multi-materials, including orthotropic and anisotropic materials, the same deduction process as shown above can be implemented to compute eigen-solutions of the associated ODEs. It is obvious that Eqs. (6) and (7) are valid for each sub-domain with a single material for analyzing the stress singularity orders near the interface tip of the dissimilar multi-material. This process will produce a set of ODEs that are similar to Eqs. (6), (7), (9) and (10). By solving the eigenvalue problem of the ODEs, the singularity orders and the associated eigen-functions near the notch tip of the dissimilar multi-materials are then determined.

To determine the stress singularities of the V-notch as described above, the ODEs need to be solved first. Niu (1993) proposed a numerical solution called *interpolating matrix method* that can solve the eigenvalue problem of ODEs effectively. By the interpolating matrix method, an interval $[\theta_1, \theta_2]$ is divided into n subintervals with $(n+1)$ divisions. All the unknown functions in the ODEs are approximated with piecewise polynomial interpolation within each of the subintervals. The highest derivatives at the division points, appearing in the ODEs, are chosen as the basic unknowns of the discrete ODEs system. The interpolating matrix method has two distinct advantages: (1) all functions and their derivatives appearing in the BVPs of ODEs are simultaneously obtained with the same degree of accuracy. This feature is particularly beneficial to the calculation of stress field that requires the first derivative of the displacement functions; (2) it can solve a general eigenvalue problems of ODEs and is convenient to write a general-purpose computer program.

Generally, in the case of $\alpha < 180°$, there exist one or several stress singularity orders λ_k in the range of $Re(\lambda_k) \in (-1, 0)$ for a V-notch problem of dissimilar multi-material.

3. The BE analysis of the stress fields and SIFs for the plane notch structures

For a plane notch structure, the displacement components in the vicinity of the notch tip can be expressed with the following expansion as (Yosibash and Szabó, 1996)

$$\begin{cases} u_\rho(\rho,\theta) = \sum_{k=1}^{N} A_k \rho^{\lambda_k+1} \tilde{u}_{\rho k}(\theta) \\ u_\theta(\rho,\theta) = \sum_{k=1}^{N} A_k \rho^{\lambda_k+1} \tilde{u}_{\theta k}(\theta) \end{cases} \tag{11}$$

where A_k ($k = 1,2,\ldots,N$) are the associated amplitude coefficients with dimension $\mathrm{mm}^{-\lambda_k}$; N is the truncated number of the eigenvalues. The A_k corresponding to the eigen-pairs of $Re(\lambda_k) \in (-1,0)$ are equivalent to the generalized stress intensity factors of the V-notch. In general, the more terms Eq. (11) takes, the bigger is the region around the notch tip that is valid for the displacement solution described by Eq. (11). The eigenvalues λ_k and the associated A_k, $\tilde{u}_{\rho k}(\theta)$, $\tilde{u}_{\theta k}(\theta)$ ($k = 1,\ldots,N$) are usually complex and can be obtained by solving Eqs. (6), (7), (9), (10). The solutions can be expressed by

$$\begin{cases} \lambda_k = \lambda_{kR} \pm i\lambda_{kI} \\ A_k = A_{kR} \pm iA_{kI} \\ \tilde{u}_{\rho k}(\theta) = \tilde{u}_{\rho kR}(\theta) \pm i\tilde{u}_{\rho kI}(\theta) \\ \tilde{u}_{\theta k}(\theta) = \tilde{u}_{\theta kR}(\theta) \pm i\tilde{u}_{\theta kI}(\theta) \end{cases} \tag{12}$$

where $i = \sqrt{-1}$; subscripts "R" and "I" represent the real and imaginary parts of a complex variable or function, respectively. After introducing Eq. (12) into Eq. (11), the displacement components $u_\rho(\rho,\theta)$,$u_\theta(\rho,\theta)$ are obtained by taking the real parts as follows:

$$\begin{aligned} \begin{Bmatrix} u_\rho(\rho,\theta) \\ u_\theta(\rho,\theta) \end{Bmatrix} = \sum_{k=1}^{N} \rho^{\lambda_{kR}+1} \Bigg\{ A_{kR} \Bigg[\begin{Bmatrix} \tilde{u}_{\rho kR}(\theta) \\ \tilde{u}_{\theta kR}(\theta) \end{Bmatrix} \cos(\lambda_{kI} \ln \rho) \\ - \begin{Bmatrix} \tilde{u}_{\rho kI}(\theta) \\ \tilde{u}_{\theta kI}(\theta) \end{Bmatrix} \sin(\lambda_{kI} \ln \rho) \Bigg] - A_{kI} \Bigg[\begin{Bmatrix} \tilde{u}_{\rho kR}(\theta) \\ \tilde{u}_{\theta kR}(\theta) \end{Bmatrix} \sin(\lambda_{kI} \ln \rho) \\ + \begin{Bmatrix} \tilde{u}_{\rho kI}(\theta) \\ \tilde{u}_{\theta kI}(\theta) \end{Bmatrix} \cos(\lambda_{kI} \ln \rho) \Bigg] \Bigg\} \end{aligned} \tag{13}$$

Considering Eqs. (2) and (3), the stress components in the vicinity of the notch tip are denoted also by the asymptotic expansion as follows:

$$\begin{cases} \sigma_\rho(\rho,\theta) = \sum_{k=1}^{N} A_k \rho^{\lambda_k} \tilde{\sigma}_{\rho k}(\theta) \\ \sigma_\theta(\rho,\theta) = \sum_{k=1}^{N} A_k \rho^{\lambda_k} \tilde{\sigma}_{\theta k}(\theta) \\ \sigma_{\rho\theta}(\rho,\theta) = \sum_{k=1}^{N} A_k \rho^{\lambda_k} \tilde{\sigma}_{\rho\theta k}(\theta) \end{cases} \tag{14}$$

Inserting Eq. (12) into Eq. (3) yields

$$\begin{cases} \tilde{\sigma}_{\rho k}(\theta) = \tilde{\sigma}_{\rho kR}(\theta) + i\tilde{\sigma}_{\rho kI}(\theta) = \frac{E}{1-\nu^2} \{ [(1+\nu)\tilde{u}_{\rho kR} + \lambda_{kR}\tilde{u}_{\rho kR} - \lambda_{kI}\tilde{u}_{\rho kI} + \nu\tilde{u}'_{\theta kR}] \\ \qquad + i[(1+\nu)\tilde{u}_{\rho kI} + \lambda_{kI}\tilde{u}_{\rho kR} + \lambda_{kR}\tilde{u}_{\rho kI} + \nu\tilde{u}'_{\theta kI}] \} \\ \tilde{\sigma}_{\theta k}(\theta) = \tilde{\sigma}_{\theta kR}(\theta) + i\tilde{\sigma}_{\theta kI}(\theta) = \frac{E}{1-\nu^2} \{ [(1+\nu)\tilde{u}_{\rho kR} + \nu\lambda_{kR}\tilde{u}_{\rho kR} - \nu\lambda_{kI}\tilde{u}_{\rho kI} + \tilde{u}'_{\theta kR}] \\ \qquad + i[(1+\nu)\tilde{u}_{\rho kI} + \nu\lambda_{kR}\tilde{u}_{\rho kI} + \nu\lambda_{kI}\tilde{u}_{\rho kR} + \tilde{u}'_{\theta kI}] \} \\ \tilde{\sigma}_{\rho\theta k}(\theta) = \tilde{\sigma}_{\rho\theta kR}(\theta) + i\tilde{\sigma}_{\rho\theta kI}(\theta) = \frac{E}{2(1+\nu)} \left[\left(\lambda_{kR}\tilde{u}_{\theta kR} - \lambda_{kI}\tilde{u}_{\theta kI} + \tilde{u}'_{\rho kR} \right) + i\left(\lambda_{kI}\tilde{u}_{\theta kR} + \lambda_{kI}\tilde{u}_{\theta kR} + \tilde{u}'_{\rho kI} \right) \right] \end{cases} \tag{15}$$

Substituting Eqs. (12) and (15) into Eq. (14), then taking the real parts of $\sigma_\rho(\rho,\theta)$, $\sigma_\theta(\rho,\theta)$ and $\sigma_{\rho\theta}(\rho,\theta)$, respectively, one obtains the following stress components:

$$\begin{aligned} \begin{Bmatrix} \sigma_\rho(\rho,\theta) \\ \sigma_\theta(\rho,\theta) \\ \sigma_{\rho\theta}(\rho,\theta) \end{Bmatrix} = \sum_{k=1}^{N} \rho^{\lambda_{kR}} \Bigg\{ A_{kR} \Bigg[\begin{Bmatrix} \tilde{\sigma}_{\rho kR}(\theta) \\ \tilde{\sigma}_{\theta kR}(\theta) \\ \tilde{\sigma}_{\rho\theta kR}(\theta) \end{Bmatrix} \cos(\lambda_{kI} \ln \rho) \\ - \begin{Bmatrix} \tilde{\sigma}_{\rho kI}(\theta) \\ \tilde{\sigma}_{\theta kI}(\theta) \\ \tilde{\sigma}_{\rho\theta kI}(\theta) \end{Bmatrix} \sin(\lambda_{kI} \ln \rho) \Bigg] - A_{kI} \Bigg[\begin{Bmatrix} \tilde{\sigma}_{\rho kR}(\theta) \\ \tilde{\sigma}_{\theta kR}(\theta) \\ \tilde{\sigma}_{\rho\theta kR}(\theta) \end{Bmatrix} \sin(\lambda_{kI} \ln \rho) \\ + \begin{Bmatrix} \tilde{\sigma}_{\rho kI}(\theta) \\ \tilde{\sigma}_{\theta kI}(\theta) \\ \tilde{\sigma}_{\rho\theta kI}(\theta) \end{Bmatrix} \cos(\lambda_{kI} \ln \rho) \Bigg] \Bigg\} \end{aligned} \tag{16}$$

In order to combine the above solution with the solution in the region Ω', the above displacement and stress components are transformed into a global Cartesian coordinate system. On the boundary Γ_R (see Fig. 2(b)), $\bar{u}_i$, $\bar{t}_i$ ($i = 1,2$) are used to denote the displacement and traction components in the Cartesian coordinate system, ox_1x_2, respectively. The transformation of the displacements and tractions from the polar coordinate system to the Cartesian coordinate system is shown below:

$$\begin{Bmatrix} \bar{u}_1 \\ \bar{u}_2 \end{Bmatrix} = \begin{bmatrix} \cos\theta & -\sin\theta \\ \sin\theta & \cos\theta \end{bmatrix} \begin{Bmatrix} u_\rho \\ u_\theta \end{Bmatrix} \tag{17}$$

$$\begin{Bmatrix} \bar{t}_1 \\ \bar{t}_2 \end{Bmatrix} = \begin{bmatrix} \cos\theta & -\sin\theta \\ \sin\theta & \cos\theta \end{bmatrix} \begin{Bmatrix} t_\rho \\ t_\theta \end{Bmatrix} = \begin{bmatrix} \cos\theta & -\sin\theta \\ \sin\theta & \cos\theta \end{bmatrix} \begin{Bmatrix} \sigma_\rho \\ \sigma_{\rho\theta} \end{Bmatrix} \tag{18}$$

Comparing Fig. 2(a) with Fig. 2(b), it can be easily seen that Γ_R and Γ'_R share the same interface. Assuming that u_i, t_i ($i = 1,2$) are defined as the displacement and traction components on Γ'_R in the coordinate system, ox_1x_2, the conditions of the perfectly bonded interface yield

$$u_i = \bar{u}_i, \quad t_i = -\bar{t}_i, \quad (\rho,\theta) \text{ on } \Gamma'_R \tag{19}$$

Substituting Eqs. (13) and (16) into Eqs. (17)–(19), u_i and t_i on Γ'_R are given as below:

$$\begin{aligned} \begin{Bmatrix} u_1 \\ u_2 \end{Bmatrix} = \sum_{K=1}^{N} \rho^{\lambda_{kR}+1} \Bigg\{ A_{kR} \Bigg[\begin{Bmatrix} \tilde{u}_{\rho kR}(\theta)\cos\theta - \tilde{u}_{\theta kR}(\theta)\sin\theta \\ \tilde{u}_{\rho kR}(\theta)\sin\theta + \tilde{u}_{\theta kR}(\theta)\cos\theta \end{Bmatrix} \cos(\lambda_{kI}\ln\rho) \\ - \begin{Bmatrix} \tilde{u}_{\rho kI}(\theta)\cos\theta - \tilde{u}_{\theta kI}(\theta)\sin\theta \\ \tilde{u}_{\rho kI}(\theta)\sin\theta + \tilde{u}_{\theta kI}(\theta)\cos\theta \end{Bmatrix} \sin(\lambda_{kI}\ln\rho) \Bigg] \\ - A_{kI} \Bigg[\begin{Bmatrix} \tilde{u}_{\rho kR}(\theta)\cos\theta - \tilde{u}_{\theta kR}(\theta)\sin\theta \\ \tilde{u}_{\rho kR}(\theta)\sin\theta + \tilde{u}_{\theta kR}(\theta)\cos\theta \end{Bmatrix} \sin(\lambda_{kI}\ln\rho) \\ + \begin{Bmatrix} \tilde{u}_{\rho kI}(\theta)\cos\theta - \tilde{u}_{\theta kI}(\theta)\sin\theta \\ \tilde{u}_{\rho kI}(\theta)\sin\theta + \tilde{u}_{\theta kI}(\theta)\cos\theta \end{Bmatrix} \cos(\lambda_{kI}\ln\rho) \Bigg] \Bigg\} \end{aligned} \tag{20}$$

$$\begin{aligned} \begin{Bmatrix} t_1 \\ t_2 \end{Bmatrix} = \sum_{K=1}^{N} \rho^{\lambda_{kR}} \Bigg\{ -A_{kR} \Bigg[\begin{Bmatrix} \tilde{\sigma}_{\rho kR}(\theta)\cos\theta - \tilde{\sigma}_{\rho\theta kR}(\theta)\sin\theta \\ \tilde{\sigma}_{\rho kR}(\theta)\sin\theta + \tilde{\sigma}_{\rho\theta kR}(\theta)\cos\theta \end{Bmatrix} \cos(\lambda_{kI}\ln\rho) \\ + \begin{Bmatrix} \tilde{\sigma}_{\rho kI}(\theta)\cos\theta - \tilde{\sigma}_{\rho\theta KI}(\theta)\sin\theta \\ \tilde{\sigma}_{\rho kI}(\theta)\sin\theta + \tilde{\sigma}_{\rho\theta kI}(\theta)\cos\theta \end{Bmatrix} \sin(\lambda_{kI}\ln\rho) \Bigg] \\ + A_{kI} \Bigg[\begin{Bmatrix} \tilde{\sigma}_{\rho kR}(\theta)\cos\theta - \tilde{\sigma}_{\rho\theta kR}(\theta)\sin\theta \\ \tilde{\sigma}_{\rho kR}(\theta)\sin\theta + \tilde{\sigma}_{\rho\theta kR}(\theta)\cos\theta \end{Bmatrix} \sin(\lambda_{kI}\ln\rho) \\ - \begin{Bmatrix} \tilde{\sigma}_{\rho kI}(\theta)\cos\theta - \tilde{\sigma}_{\rho\theta kI}(\theta)\sin\theta \\ \tilde{\sigma}_{\rho kI}(\theta)\sin\theta + \tilde{\sigma}_{\rho\theta kI}(\theta)\cos\theta \end{Bmatrix} \cos(\lambda_{kI}\ln\rho) \Bigg] \Bigg\} \end{aligned} \tag{21}$$

Thus, the displacements u_i and tractions t_i on the inner boundary Γ'_R of the remaining region Ω' (see Fig. 2(a)) are represented by the solutions of the eigen-analysis of the ODEs in Section 2.

To determine the displacement and stress fields of the plane V-notched structure, the new technique proposed here requires division of the regions Ω' and Ω_R as shown in Fig. 2. Firstly, the solutions of the stress singularities in the small sector Ω_R are evaluated by analyzing the eigenvalue problem of the ODEs shown by Eqs. (6) and (7) and the boundary conditions of Eq. (9) and (10). In the present paper, the interpolating matrix method (Niu, 1993) is adopted to solve the ODEs, which can provide the solutions of the top N dominant singularities, including $\lambda_k, \tilde{u}_{\rho k}(\theta), \tilde{u}_{\theta k}(\theta)$, $\tilde{\sigma}_{\rho k}(\theta), \tilde{\sigma}_{\theta k}(\theta)$ and $\tilde{\sigma}_{\rho\theta k}(\theta)$ $(k = 1,\ldots,N)$. Note that A_{kR} and A_{kI},$(k = 1,\ldots,N)$ in Eqs. (20) and (21) are unknown quantities that will be determined in the next step.

Let us consider now the remaining region Ω' (see Fig. 2(a)). There is no stress singularity in Ω'. Therefore the conventional BEM is capable of analyzing the part described by Ω' without other special treatment. The boundary $\Gamma' + \Gamma'_1 + \Gamma'_2 + \Gamma'_R$ of Ω' is divided into meshes. The boundary integral equation is written as follows:

$$C_{ij}(\boldsymbol{y})u_j(\boldsymbol{y}) = \int_\Gamma U^*_{ij}(\boldsymbol{x},\boldsymbol{y})t_j(\boldsymbol{x})\,d\Gamma - \int_\Gamma T^*_{ij}(\boldsymbol{x},\boldsymbol{y})u_j(\boldsymbol{x})\,d\Gamma + \int_\Omega U^*_{ij}(\boldsymbol{x},\boldsymbol{y})b_j(\boldsymbol{x})\,d\Omega, \quad \boldsymbol{y}\in\partial\Omega' \tag{22}$$

where $\boldsymbol{y}$ is the source (load) point; $\boldsymbol{x}$ the field point; b_j is the body force per unit volume; u_j and t_j $(i = 1,2)$ are, respectively, the displacements and tractions on $\Gamma' + \Gamma'_1 + \Gamma'_2 + \Gamma'_R$. $U^*_{ij}(\boldsymbol{x},\boldsymbol{y})$ and $T^*_{ij}(\boldsymbol{x},\boldsymbol{y})$ are the Kelvin displacement and traction fundamental solutions. $\int(\cdots)d\Gamma$ denotes the Cauchy principal value integral. The $C_{ij}(\boldsymbol{y})$ are known coefficients, the values of which depend on the geometric configuration and material property around a source point $\boldsymbol{y}$. The coefficients are calculated by

$$\left[C_{ij}(\boldsymbol{y})\right]_{2\times2} = \frac{1}{2\pi}\begin{bmatrix} \varphi - \frac{1+\nu}{4}(\sin2\alpha_2 - \sin2\alpha_1) & \frac{1+\nu}{4}(\cos2\alpha_2 - \cos2\alpha_1) \\ \frac{1+\nu}{4}(\cos2\alpha_2 - \cos2\alpha_1) & \varphi + \frac{1+\nu}{4}(\sin2\alpha_2 - \sin2\alpha_1) \end{bmatrix}$$

where the angles φ, α_1, α_2 are defined in Fig. 3; $C_{ij}(\boldsymbol{y}) = \delta_{ij}$ for internal points and $C_{ij}(\boldsymbol{y}) = 0.5\delta_{ij}$ for smooth boundary points; δ_{ij} is the Kronecker delta. For a plane strain problem of an isotropic homogeneous medium, the fundamental solutions are

$$U^*_{ij} = \frac{-1}{8\pi(1-\nu)G}\left[(3-4\nu)\ln r\delta_{ij} - r_{,i}r_{,j}\right] \tag{23}$$

$$T^*_{ij} = \frac{1}{4\pi(1-\nu)r}\left\{(1-2\nu)(r_{,i}n_j - r_{,j}n_i) - r_{,n}\left[(1-2\nu)\delta_{ij} + 2r_{,i}r_{,j}\right]\right\} \tag{24}$$

where G is the shear modulus; y_i and x_i denote the Cartesian coordinate components of $\boldsymbol{y}$ and $\boldsymbol{x}$, respectively. n_i denotes the unit outward normal vector on the boundary. Hence we can write

$$r_{,i} = \frac{\partial r}{\partial x_i} = \frac{r_i}{r}, \quad r_{,n} = \frac{\partial r}{\partial n} = r_{,i}n_i, \qquad r_i = x_i - y_i,\ r = \sqrt{r_i r_i} \tag{25}$$

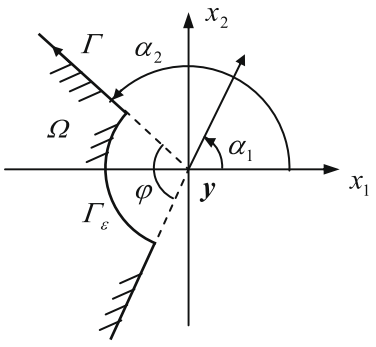

Fig. 3. Geometric configuration around a source point $\boldsymbol{y}$ on boundary.

Note that for the region $\Omega', \Gamma' + \Gamma'_1 + \Gamma'_2$ is the outer boundary of the notch structure and Γ'_R is an inner boundary which arises from the separation of the regions Ω' and Ω_R. M nodes are generated on $\Gamma' + \Gamma'_1 + \Gamma'_2$ from the division for the BE analysis and n points are chosen on Γ'_R for the interpolating matrix method. The nodal displacements and tractions at all the nodes on $\Gamma' + \Gamma'_1 + \Gamma'_2$ are expressed, respectively, by the displacement vector $\boldsymbol{U} = (u_{x_1 1}\ u_{x_2 1}\ u_{x_1 2}\ u_{x_2 2}\cdots u_{x_1 M}\ u_{x_2 M})^T$ and the traction vector $\boldsymbol{T} = (t_{x_1 1}\ t_{x_2 1}\ t_{x_1 2}\ t_{x_2 2}\cdots\ t_{x_1 M}\ t_{x_2 M})^T$. The displacements and tractions at the n interpolation points on Γ'_R have been given by Eqs. (20) and (21). The λ_k and the values of $\tilde{u}_{\rho k}(\theta)$, $\tilde{u}_{\theta k}(\theta), \tilde{\sigma}_{\rho k}(\theta), \tilde{\sigma}_{\theta k}(\theta)$ and $\tilde{\sigma}_{\rho\theta k}(\theta)$ $(k = 1,\ldots,N)$ at the n points on Γ'_R have been obtained from the previous eigen-solutions of Eqs. (6), (7) and (9), (10) by using the interpolating matrix method with the A_{kR}, A_{kI} $(k = 1,\ldots,N)$ remaining as unknowns. The amplitude coefficients in Eq. (11) are the components of vector $\boldsymbol{A} = (A_{1R}A_{1I}A_{2R}A_{2I}\cdots A_{NR}A_{NI})^T$.

It is well known that the BEM is a technique to transform the boundary integral equation into a set of algebraic equations. After Eq. (22) is discretized by the boundary elements on $\Gamma' + \Gamma'_1 + \Gamma'_2 + \Gamma'_R$, any unknown functions in Eq. (22), such as $u_i(\boldsymbol{x}), t_i(\boldsymbol{x})$, $U^*_{ij}(\boldsymbol{x},\boldsymbol{y})$ and $T^*_{ij}(\boldsymbol{x},\boldsymbol{y})$, can be approximated with piecewise polynomial shape functions multiplied by nodal values of the functions along the boundary. At each load point $\boldsymbol{y}$, the integration of Eq. (22) with respect to $\boldsymbol{x}$ over all the elements leads to two algebraic equations for a two-dimensional problem. Letting each of the M nodes on $\Gamma' + \Gamma'_1 + \Gamma'_2$ act as the load point in applying Eq. (22) for the region, Ω', in turns, the following 2 M algebraic equations are obtained

$$\begin{bmatrix}\mathbf{H}_{bb} & \mathbf{H}_{b\rho}\end{bmatrix}\begin{Bmatrix}\mathbf{U}\\ \mathbf{A}\end{Bmatrix} = \begin{bmatrix}\mathbf{G}_{bb} & \mathbf{G}_{b\rho}\end{bmatrix}\begin{Bmatrix}\mathbf{T}\\ \mathbf{A}\end{Bmatrix} \tag{26}$$

where $\mathbf{H}_{bb}$, $\mathbf{H}_{bp}$, $\mathbf{G}_{bb}$ and $\mathbf{G}_{bp}$ are constant coefficient matrices. In a well-posed problem either the displacement, or the traction, or a combination of the two at the x_i-direction of each node is prescribed on the boundary. Therefore in the vectors $\mathbf{U}$ and $\mathbf{T}$ of Eq. (26) there are 2 M known and 2 M unknown quantities, respectively. Considering that all the components of $\mathbf{A}$ are also unknown quantities, 2 N additional algebraic equations are required to determine the vectors $\mathbf{A}$, $\mathbf{U}$ and $\mathbf{T}$. To this end, the N points from the uniform division on the inner boundary Γ'_R are chosen as the source points to apply the boundary integral equation Eq. (22) for the region Ω'. Thus the following 2N algebraic equations are established:

$$\begin{bmatrix}\mathbf{H}_{\rho b} & \mathbf{H}_{\rho\rho}\end{bmatrix}\begin{Bmatrix}\mathbf{U}\\ \mathbf{A}\end{Bmatrix} = \begin{bmatrix}\mathbf{G}_{\rho b} & \mathbf{G}_{\rho\rho}\end{bmatrix}\begin{Bmatrix}\mathbf{T}\\ \mathbf{A}\end{Bmatrix} \tag{27}$$

where $\mathbf{H}_{\rho b}$, $\mathbf{H}_{\rho p}$, $\mathbf{G}_{\rho b}$ and $\mathbf{G}_{\rho p}$ are also constant coefficient matrices.

The combination of Eqs. (26) and (27) gives

$$\begin{bmatrix}\mathbf{H}_{bb} & \mathbf{H}_{b\rho}\\ \mathbf{H}_{\rho b} & \mathbf{H}_{\rho\rho}\end{bmatrix}\begin{Bmatrix}\mathbf{U}\\ \mathbf{A}\end{Bmatrix} = \begin{bmatrix}\mathbf{G}_{bb} & \mathbf{G}_{b\rho}\\ \mathbf{G}_{\rho b} & \mathbf{G}_{\rho\rho}\end{bmatrix}\begin{Bmatrix}\mathbf{T}\\ \mathbf{A}\end{Bmatrix} \tag{28}$$

Eq. (28) is a set of $2(M+N)$ algebraic equations with $2(M+N)$ unknown quantities. The solutions of Eq. (28) give all the nodal displacements u_i and tractions t_i on $\Gamma' + \Gamma'_1 + \Gamma'_2 + \Gamma'_R$ and the amplitude coefficients A_{kR}, A_{kI} $(k = 1,\ldots,N)$.

Next, by substituting A_{kR} and A_{kI} into Eqs. (13), (16), the displacement and stress distributions in the vicinity of the notch tip are found. The displacements and stresses at any inner point $\boldsymbol{y}$ in the region Ω' can be calculated, respectively, by Eq. (22) and the following stress integral equation:

$$\sigma_{ij}(\boldsymbol{y}) = \int_\Gamma \left[W^*_{ijk}(\boldsymbol{x},\boldsymbol{y})t_k(\boldsymbol{x}) - S^*_{ijk}(\boldsymbol{x},\boldsymbol{y})u_k(\boldsymbol{x})\right]d\Gamma + \int_\Omega W^*_{ijk}b_k(\boldsymbol{x})\,d\Omega, \quad \boldsymbol{y}\ \text{in}\ \Omega' \tag{29}$$

where the kernel functions W^*_{ijk} and S^*_{ijk} are linear combinations of the derivatives of $U^*_{ij}(\boldsymbol{x},\boldsymbol{y})$ and $T^*_{ij}(\boldsymbol{x},\boldsymbol{y})$ with respect to $\boldsymbol{y}$.

Finally, from the obtained amplitude coefficients A_{kR}, A_{kI} ($k = 1, \ldots, N$) and the stress solutions of Eq. (16) or stress eigen-functions $\tilde{\sigma}_{ij}(\theta)$, the notch stress intensity factors K_i can be determined as follows.

When λ_1 and λ_2 are real numbers,

$$K_{\mathrm{I}} = \lim_{\rho\to 0}\sqrt{2\pi}\rho^{-\lambda_1}\sigma_\theta(\rho,\theta)|_{\theta=0} = \sqrt{2\pi}A_1\tilde{\sigma}_{\theta 1}(0) \tag{30a}$$

$$K_{\mathrm{II}} = \lim_{\rho\to 0}\sqrt{2\pi}\rho^{-\lambda_2}\sigma_{\rho\theta}(\rho,\theta)|_{\theta=0} = \sqrt{2\pi}A_2\tilde{\sigma}_{\rho\theta 2}(0) \tag{30b}$$

When λ_1 is a complex number (Rice, 1988),

$$\begin{aligned} K_{\mathrm{I}} + iK_{\mathrm{II}} &= \lim_{\rho\to 0}\sqrt{2\pi}\rho^{-\lambda_{1\mathrm{R}}-i\lambda_{1\mathrm{I}}}\left[\sigma_\theta(\rho,\theta)+i\sigma_{\rho\theta}(\rho,\theta)\right]|_{\theta=0} \\ &= \sqrt{2\pi}\,(A_{1\mathrm{R}}+iA_{1\mathrm{I}})\left[\tilde{\sigma}_{\theta 1\mathrm{R}}(0)-\tilde{\sigma}_{\rho\theta 1\mathrm{I}}(0)+i(\tilde{\sigma}_{\theta 1\mathrm{I}}(0)+\tilde{\sigma}_{\rho\theta 1\mathrm{R}}(0))\right] \\ &= \sqrt{2\pi}\left[A_{1\mathrm{R}}(\tilde{\sigma}_{\theta 1\mathrm{R}}(0)-\tilde{\sigma}_{\rho\theta 1\mathrm{I}}(0))-A_{1\mathrm{I}}(\tilde{\sigma}_{\theta 1\mathrm{I}}(0)+\tilde{\sigma}_{\rho\theta 1\mathrm{R}}(0))\right] \\ &\quad + i\sqrt{2\pi}\left[A_{1R}(\tilde{\sigma}_{\theta 1\mathrm{I}}(0)+\tilde{\sigma}_{\rho\theta 1\mathrm{R}}(0))+A_{1\mathrm{I}}(\tilde{\sigma}_{\theta 1R}(0)-\tilde{\sigma}_{\rho\theta 1\mathrm{I}}(0)\right] \end{aligned} \tag{31}$$

The notch SIFs represent the strength of the singularity at the sharp notch tip and are the important parameters of interest.

4. Numerical examples

Example 1. Consider a V-notch plate of isotropic material under uniaxial tension as shown in Fig. 4(a).

The plate is in plane stress state with $h = 200$ mm, $w = 40$ mm, Young's modulus $E = 3.9 \times 10^9$ Pa, Poisson's ratio $v = 0.25$ and load $\sigma = 1$ MPa. The opening angle γ and the depth l of the notch are variable. First, the routine IMMEI of the interpolating matrix method is used to evaluate the stress singularity orders and the associated eigen-functions around the notch tip. Referring to Eqs. (6), (7) and Fig. 4(b) where Γ_R and Γ_R' are a pair of fictitious boundaries, interval $[\theta_1, \theta_2]$ is divided into n uniform subintervals. The eigenvalues are complex and are expressed by $\lambda_k = \xi_k \pm i\eta_k$. For $\gamma = 60°$, Tables 1 and 2 present the first 13 eigenvalues whose $Re(\lambda_k)$, i.e., ξ_k, are larger than or equal to -1. Note that the conjugate values and $\lambda_k = -1$ are not listed in the tables. The eigenvalues in Tables 1 and 2 are, respectively, corresponding to the mode I (opening) and mode II (sliding) eigen-functions $\tilde{u}_\rho(\theta)$. Comparisons are made with Fu and Long's results (2003) that were obtained from the sub-region accelerated Müller method for the characteristic equation derived by Williams (1952). The results of Seweryn (2002), obtained using a special FEM in conjunction with an analytical stress expression, are also shown in the tables for comparisons. To obtain Seweryn's results, half of the notch structure, due to symmetry, was discretized with 152 six-node triangular elements.

It can be seen in Tables 1 and 2 that the eigenvalues obtained using the present method approach the results of Fu and Long (1998) as n increases. The two eigenvalues in the range of $-1 < \lambda_k < 0$ for $n = 80$ have converged up to the fifth significant figure. In addition, the associated eigenvectors $\tilde{u}_{\rho k}(\theta), \tilde{u}_{\theta k}(\theta), \tilde{\sigma}_{\rho k}(\theta), \tilde{\sigma}_{\theta k}(\theta)$ and $\tilde{\sigma}_{\rho\theta k}(\theta)$ are simultaneously obtained with the same degree of accuracy by the IMMEI.

The BEM is adopted next to analyze the remaining structure (Fig. 4(c)) excluding the small sector around the notch tip (Fig. 4(b)). The boundary $\Gamma' + \Gamma_1' + \Gamma_2'$ of the remaining structure is divided by 80 iso-parametric quadratic elements with 160 nodes. The fictitious boundary Γ_R' is divided by 48 iso-parametric quadratic elements with 96 nodes, where the displacements and tractions at all the nodes on Γ_R' have been represented by Eqs. (20) and (21) through Eq. (19). To test the effectiveness of the pres-

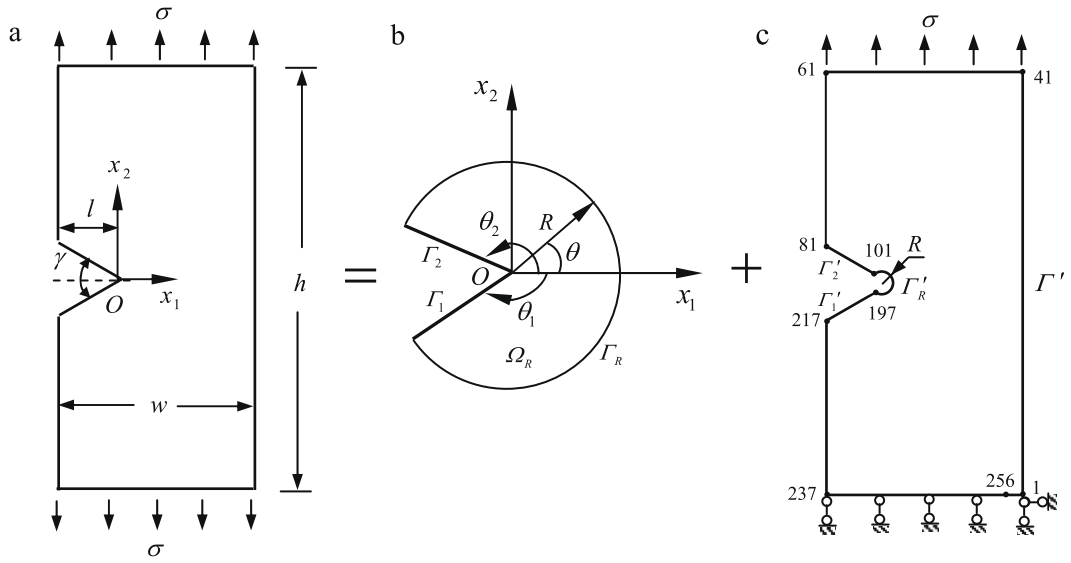

Fig. 4. A symmetrical V-notched plate under uniaxial tension load. (a) Geometry of the notch plate. (b) Sub-domain of radius R around the notch tip. (c) BE mesh division along the boundary of the remaining structure.

Table 1
The eigenvalues λ_k of the mode I eigen-functions $\tilde{u}_\rho(\theta)$, $\gamma = 60°$.

Methods	ξ_1	η_1	ξ_2	η_2	ξ_3	η_3	ξ_4	η_4
Fu (2003)	−0.487779	0	0.471028	0.141853	1.677615	0.284901	2.881487	0.360496
Seweryn (2002)	−0.4878	0	0.4710	0.1418	1.6776	0.2849		
IMMEI, $n = 20$	−0.487717	0	0.471813	0.143640	1.684805	0.296623	2.924016	0.408020
IMMEI, $n = 40$	−0.487775	0	0.471073	0.141991	1.678017	0.285650	2.883292	0.363632
IMMEI, $n = 80$	−0.487778	0	0.471035	0.141869	1.677673	0.284994	2.881766	0.360853

Table 2
The eigenvalues λ_k of the mode II eigen-functions $\tilde{u}_\rho(\theta)$, $\gamma = 60°$.

Methods	ξ_1	η_1	ξ_2	η_2	ξ_3	η_3	ξ_4	η_4
Fu (2003)	−0.269099	0	0	0	1.074826	0.229426	2.279767	0.326690
Seweryn (2002)	−0.2691	0	0	0	1.0749	0.2294		
IMMEI, $n = 20$	−0.268710	0	0	0	1.077382	0.234207	2.297998	0.351998
IMMEI, $n = 40$	−0.269070	0	0	0	1.075014	0.229741	2.280884	0.328306
IMMEI, $n = 80$	−0.269095	0	0	0	1.074848	0.229466	2.279900	0.326881

Table 3
The stress amplitudes A_k corresponding to λ_k when $\gamma = 60°$, $l/w = 0.2$, $R/l = 0.001$.

k	1	2	3	4	5	6	7	8
A_{kR} ($mm^{-\lambda_k}$)	2.51E−09	5.17E−12	1.31E−09	4.80E−10	−7.94E−07	−2.56E−06	1.13E−04	−3.51E−04
A_{kI} ($mm^{-\lambda_k}$)	0.00E+00	0.00E+00	−4.03E−10	−8.41E−09	1.37E−06	−2.35E−06	4.55E−04	9.72E−04

Table 4
The notch SIF $K_I/(N\ mm^{-2-\lambda_1})$ viz different R and N ($\gamma = 60°$, $l/w = 0.2$).

	N (%)							
R/l	2	4	6	8	10	12	14	16
K_I								
0.1	7.0615	7.0154	7.0337	7.0664	7.0347	7.0194	7.0335	7.0580
0.3	7.0739	7.0269	7.0404	7.0581	7.0411	7.0303	7.0397	7.0299
0.5	6.9988	7.0469	7.0678	7.0698	7.0684	7.1124	7.1120	7.1059
0.7	7.0975	7.0451	7.0563	7.0688	7.0574	7.0509	7.0560	7.0553
0.9	7.1016	7.0447	7.0562	7.0655	7.0572	7.0520	7.0565	7.0562
1.1	7.1054	7.0510	7.0565	7.0666	7.0577	7.0527	7.0569	7.0575
1.3	7.1089	7.0537	7.0572	7.0653	7.0580	7.0536	7.0572	7.0584
1.5	6.9805	7.0328	7.0442	7.0522	7.0408	7.0266	7.0323	7.0235
1.7	7.0129	7.0388	7.0423	7.0567	7.0407	7.0304	7.0363	7.0307
1.9	7.0345	7.0340	7.0416	7.0511	7.0445	7.0354	7.0406	7.0366
2.1	7.0609	7.0361	7.0530	7.0704	7.0567	7.0501	7.0551	7.0509

Note that $K_I = 7.0627\ N\ mm^{-2-\lambda_1}$ from Chen (1995).

ent approach, the notch plate is analyzed by choosing different radius R and number of terms, N, in the expansion. By fixing the notch depth ratio, l/w, to 0.2, the solutions are obtained for variable radius to depth ratio, R/l, between 0.1% and 2.1% and variable γ from 0° to 90°. By performing the BE analysis, the displacements and tractions on $\Gamma' + \Gamma'_1 + \Gamma'_2 + \Gamma'_R$ and the amplitude coefficients A_k are obtained. Consequently, the displacement and stress distributions in the whole region Ω are computed by Eqs. (13), (16) and (22), (29). Table 3 shows the values of $A_k = A_{kR} + iA_{kI}$ for $\gamma = 60°$, $l/w = 0.2$,$R/l = 0.1\%$ and $N = 8$.

Substituting the A_k into Eq. (30) yields the notch stress intensity factors. Table 4 shows K_I of the notch with $\gamma = 60°$ and $l/w = 0.2$ for different radius R and term number N. The results are compared with Chen's solution (1995) that was obtained by using the body force method. Due to symmetry, mode II notch SIF does not exist in this problem. This can be seen from Table 3 where the value of A_2, which is associated to K_{II}, is nearly zero in comparison with other A_k.

It is observed in Table 4 that for any fixed value of N, the SIFs are all in good agreement with the existing results (Chen, 1995). This demonstrates that the present approach is numerically stable for evaluating the stress fields of notch structures in terms of the radius R. In Table 4 we can also see that all the computed K_I by taking number $N = 2$ are very close to those obtained by taking $N \geqslant 4$. It shows that the first two terms in the asymptotic expansion of Eq. (11) dominate the singular stress field in the notch tip region for the homogeneous and isotropic material. Although higher order terms in Eq. (11) do not make significant contributions to the notch SIF of the first order, the inclusion of them in the solution is still important and can improve the accuracy of the stress solutions

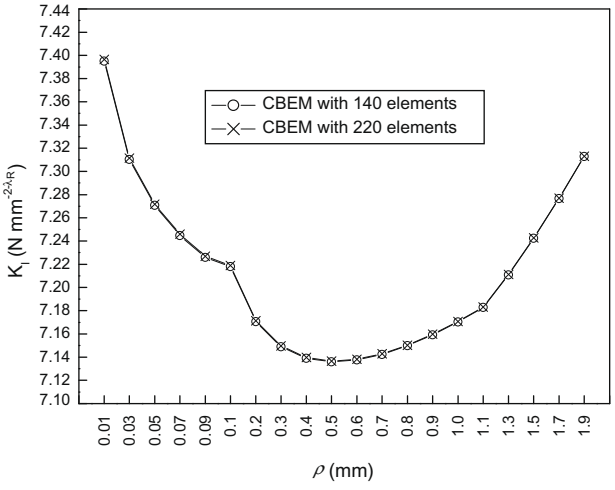

Fig. 5. The notch SIF computed by CBEM when $\gamma = 60°$, $l/w = 0.2$.

in the tip region. Especially, the higher order terms are becoming more significant in the stress expression Eq. (16) as ρ increases. In addition, notch SIFs of higher orders exist in many notch structures and have to be determined by the solutions of higher order terms. It is worth to mention that in the past studies on notch structures, only a few researchers have mentioned and dealt with higher order terms because of the analytical difficulties.

Table 4 shows also that the largest relative difference Δ of all the values of K_I obtained using the present BEM with $N \geqslant 4$ is

Table 5
The notch SIF $K_1/(\mathrm{N\,mm^{-2-\lambda_1}})$ with different l/w and γ.

l/w	$\gamma = 30°$			$\gamma = 60°$		
	Present method	Chen (1995)	Δ (%)	Present method	Chen (1995)	Δ (%)
0.05	2.8907	2.8820	0.3019	3.0084	2.9951	0.4441
0.10	4.2668	4.2486	0.4284	4.4294	4.3847	1.0195
0.20	6.8740	6.9017	0.4014	7.0501	7.0627	0.1784
0.30	10.1131	10.2462	1.299	10.3576	10.4300	0.6942
0.40	14.8843	15.0316	0.9799	15.1769	15.2365	0.3912
0.50	22.2281	22.4423	0.9544	22.5603	22.6973	0.6036
0.60	34.7102	35.0603	0.9986	35.1814	35.4083	0.6408
0.70	58.9055	59.5953	1.1575	59.5426	60.2095	1.1076

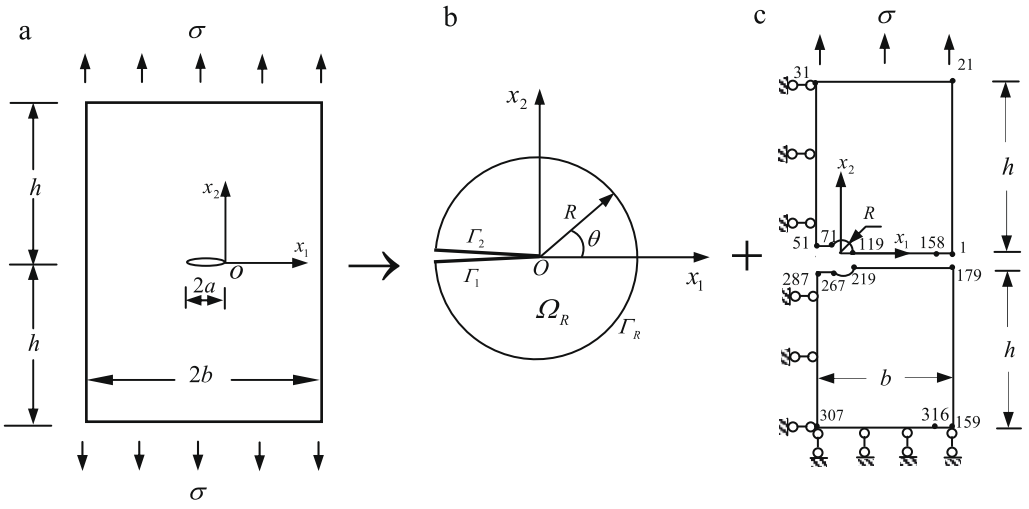

Fig. 6. A plate with a central crack under uniaxial tension load. (a) Geometry of the crack plate. (b) Sub-domain of radius R around the right crack tip. (c) BE mesh division along the boundary of the remaining structure.

0.7% in comparison with the reference solution $K_I = 7.0627\ \mathrm{N\,mm^{-2-\lambda_1}}$ (Chen, 1995). The relative difference is calculated by

$$\Delta\ (\%) = \frac{\mathrm{Solution_{Present}} - \mathrm{Solution_{Ref.}}}{\mathrm{Solution_{Ref.}}} \times 100 \tag{32}$$

In order to compare the accuracy of the present BEM with that of the conventional BEM for analyzing notch problems, the notch plate of Fig. 4(a) with $\gamma = 60°$, $l/w = 0.2$ is again considered. Without the eigen-analysis, the conventional BEM (CBEM) requires very fine meshes on the boundary of the region near the tip to model the stress distribution. The displacement and stress distributions are achieved, respectively, with 140 quadratic elements and 220 quadratic elements on the boundary of the half structure. Along the x_1-axes, the stresses at the mesh points of distance ρ measured from the tip O are substituted into Eq. 30a to determine the notch SIF. The results are plotted in Fig. 5.

It can be seen in Fig. 5 that the computed K_I from the conventional BEM varies significantly as the value of ρ changes. Only in the range of $3.75\% \leqslant \rho/l \leqslant 10\%$ the results of K_I are reliable since the conventional BEM cannot model the stress singularities in the vicinity of the notch tip. For the problem solved in Table 4, where $K_I = 7.0627\ \mathrm{N\,mm^{-2-\lambda_1}}$ (Chen, 1995), the best solution of K_I from the conventional BE analysis is $7.1390\ \mathrm{N\,mm^{-2-\lambda_1}}$ at which ρ/l is 6.25% (see Fig. 5) and the relative difference between the two solutions increases to $\Delta = 1.08\%$. Further tests, which are not shown here, confirmed that a refinement of the meshes in the tip region helped little in improving the accuracy of the results shown in Fig. 5.

Clearly, since the assumption of asymptotic expansion of the stress field can reflect the essential stress singularities near a

Table 6
The SIF $K_1(/\sigma\sqrt{\pi a})$ of the central-crack plate.

N	8	10	12
Present BEM	1.0273	1.0296	1.0297
Analytic solution	1.0263	1.0263	1.0263
Δ (%)	0.099%	0.320%	0.332%

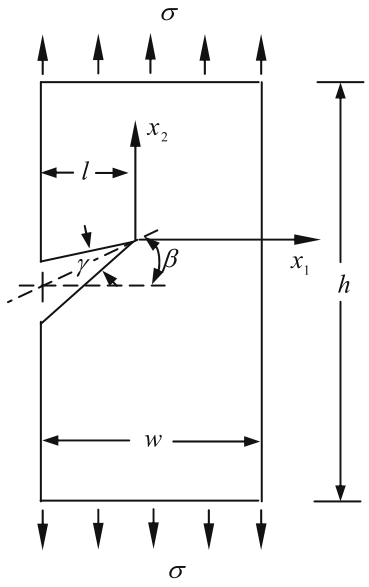

Fig. 7. A plate with an inclined V-notch under uniaxial tension load.

Table 7
The notch SIFs of the inclined V-notch plate ($l/w = 0.2$).

γ/β (°)	$K_I/(\text{N mm}^{-2-\lambda_1})$			$K_{II}/(\text{N mm}^{-2-\lambda_2})$		
	Present method	Chen (1995)	Δ (%)	Present method	Chen (1995)	Δ (%)
30/0	6.8282	6.9017	1.0650	0.0197	0.0000	/
30/15	6.6625	6.6768	0.2142	1.2065	1.2017	0.3994
30/30	6.0129	6.0471	0.5656	2.2026	2.1908	0.5386
30/45	5.0519	5.0975	0.8946	2.8522	2.8080	1.5741
60/0	7.0501	7.0627	0.1784	0.0028	0.0000	/
60/15	6.8671	6.8037	0.9318	1.2628	1.2468	1.2833
60/30	6.1173	6.0705	0.7709	2.2386	2.2239	0.6610
60/45	5.0146	4.9854	0.5857	2.6967	2.7388	1.5372

V-notch tip, the stress distributions from the present BEM are more accurate than those from the conventional BEM. It is observed that the computed notch SIF is nearly a fixed value that does not depend on the chosen radius R of the small sector. Furthermore the present BEM obtains all the amplitude coefficients A_k of the first N terms. The A_k can be used to determine the notch SIF of the k-th order together with the k-th order eigen-functions. Moreover, multiple notch SIFs can be calculated by the new method, while the conventional BEM and FEM have difficulties in dealing with this.

Table 5 shows the notch SIFs obtained using the present BEM for variable depth l and opening angle γ. $N = 12$ and $R = 0.018$ mm are taken in the calculation. It can be seen that the relative differences between the computed SIFs and Chen's solutions (1995) for all the cases are less than 1.3%.

Example 2. Consider a finite plate with a central crack under uniaxial tension as shown in Fig. 6(a).

The standard mode-I crack in an isotropic material is used to show the accuracy of the present method. The plate is in plane stress state with $2b = 2.0$ m, $2h = 3.0$ m, $2a = 0.4$ m. The material parameters and load are $E = 210$ Pa, $\nu = 0.3$ and $\sigma = 1$ MPa, respectively.

Due to symmetry, only one half of the plate is considered in the analysis, as shown in Fig. 6(b and c). After the stress singularity orders and eigenvectors of the small sector of radius R are obtained by the interpolating matrix method, the new BEM technique is adopted to evaluate the displacement and stress fields of the crack plate which is divided by two sub-domains, as shown in Fig. 6(c). In the calculation, $R/a = 1.3\%$, and $n = 96$ are taken. The boundaries of the two sub-domains are divided by 158 quadratic elements with 316 nodes. Table 6 shows the computed SIF K_I viz different term number N of the eigenvalues by using the present method. For the finite plate with mode I central-crack, an analytic solution of the SIF K_I is $1.0263\sigma\sqrt{\pi a}$ (The Aeronautical Research Institute of China, 1993). Compared with the analytical solution, the relative errors of all the results in the table are less than 0.332%.

The idea of the present method to analyze the V-notch structures is similar to one of Chen and Sze (2001). Chen and Sze (2001) used the full-field finite elements to analyze the V-notch/crack structures. In the similar case as Fig. 6(a), Chen and Sze (2001) took $2b = 2.0$ m, $2h = 2.0$ m, $2a = 0.2$ m as an infinite plate with a central crack while other parameters are the same as above. The exact solution of the SIF for the crack plate is $K_I = 1.0000\sigma\sqrt{\pi a}$. For one half of the crack plate, Chen and Sze (2001) applied 404 five-parameter 4-node elements (a special hybrid FE), one super 9-notch crack-tip element and 23 eigenvalues to evaluate the stress field of the plate and obtained $K_I = 1.0132\sigma\sqrt{\pi a}$. The relative error is 0.132%.

It can be seen that the present BEM is to apply less node number (unknown quantities) than the hybrid FEM for analyzing the notch/crack structures with the similar way.

Example 3. Consider a plate with an inclined V-notch subjected to uniaxial tension load as shown in Fig. 7

The dimensions of the plate are $h = 200$ mm, $w = 40$ mm. γ is the inclined notch angle. β is the angle between the bisector of the notch angle and the x_1-axis. The material parameters and load are $E = 3.9 \times 10^9$ Pa, $\nu = 0.373$ and $\sigma = 1$ MPa, respectively. For the sake of testing the accuracy of the results in terms of different geometric configurations, the angles γ and β and the notch depth l are taken variable. Since the notch is inclined, there exist the notch SIFs of both mode I and mode II.

After the stress singularity orders and eigenvectors of the small sector of radius R are obtained by the interpolating matrix method, the new BEM technique is adopted to evaluate the displacement and stress fields of the notch plate. In the calculation, $R = 0.018$ mm, $N = 12$ and $n = 96$ are taken. As done in Example 1, the outer boundary of the remaining region is divided into 80 quadratic elements. Table 7 shows the computed notch SIFs for $\gamma = 30°, \gamma = 60°$, $l/w = 0.2$ and different β. Chen's solutions (1995) shown in the table were obtained from the body force method. The table shows that an increase of β results in an increase of the mode II notch SIF, while a decrease of the mode I notch SIF. All the relative differences between the present results and Chen's solutions (1995) for K_I and K_{II} are less than 1.1% and 1.6%, respectively.

5. Conclusions

In conjunction with an asymptotic expansion of the stress distribution near the notch tip, a new BEM has been proposed in this paper to determine the singular stress fields of plane V-notch structures.

For a plane V-notch structure, the new method treats it as an assembly of two parts, i.e., a small sector of material around the notch tip and the remaining part of the structure. The stresses and displacements of the small sector are represented by asymptotic expansions. On the basis of the liner elasticity theory, the evaluations of the stress singularity orders and the associated displacement/stress eigen-functions were transformed into an eigenvalue problem of ordinary differential equations. The interpolating matrix method was applied to solving the eigenvalue problem with both the eigenvalues and the eigenvectors being obtained simultaneously. The displacements and tractions along the arc of the sector were expressed as a linear combination of the terms from the series expansions with different singularity orders. In fact, the small sector can be thought as a super singular element around the notch tip, and the displacement/stress eigenfunctions obtained through the eigen-analysis are essentially equivalent to a series of shape functions of the singular element for modeling the displacement/stress distribution. Since the remaining part has no stress singularities, the conventional BE is sufficiently accurate to predict the displacement and stress

distributions. A combination of the two solutions finally provided the stress fields of the sector and the remaining structure as well as the notch SIFs.

In contrast to the conventional BEM and FEM, the proposed BE approach does not require fine meshes near a V-notch tip. Another advanced feature of the new method is that, both the basic and higher order stress singularities can be revealed simultaneously through the asymptotic expansion and eigen-analysis. Using the present method, the fracture analysis of complex geometric and load conditions becomes possible and accurate.

Three numerical examples have been given to show the application of the new method on V-notch/crack plates made of isotropic materials. For V-notch plates with different geometry, the stress fields and the notch SIFs were computed for different values of the radius R and the expansion term number N. Through comparisons with alternative solutions available in the literature, it can be concluded that the new method is an accurate and effective tool for modeling singular stress fields in V-notch structures.

The present technique can be further developed to evaluate the stress distributions and the generalized SIFs of junctions, inclusions and V-notches in bonded dissimilar multi-material. In these cases, high order stress singularities are needed and can be obtained by the present method. This will make it possible for fracture criteria associated to these complex cases to be established. Future work is in progress in order to establish new fracture criteria on the basis of equivalent energy release rate of different V-notch angles.

Acknowledgments

The first two authors acknowledge the financial support from the Natural Science Foundation of Anhui Province of China (090414153). The authors are very grateful to the anonymous reviewers for their constructive comments and suggestions.

References

Atzori, B., Meneghetti, G., Susmel, L., 2002. Estimation of the fatigue strength of light alloy welds by an equivalent notch stress analysis. International Journal of Fatigue 24, 591–599.

Barsoum, R.S., 1976. On the use of isoparametric finite elements in linear fracture mechanics. International Journal for Numerical Methods in Engineering 10, 25–27.

Blandford, G.E., Ingraffea, A.R., Liggett, J.A., 1981. Two-dimensional stress intensity factor computations using the boundary element methods. International Journal for Numerical Methods in Engineering 17, 387–404.

Carpenter, W.C., 1984. Calculation of fracture mechanics parameters for a general corner. International Journal of Fracture 24, 45–48.

Carpinteri, A., Paggi, M., Pugno, N., 2006. Numerical evaluation of generalized stress-intensity factors in multi-layered composites. International Journal of Solids and Structures 43, 627–641.

Chen, D.H., 1995. Stress intensity factors for V-notched strip under tension or in-plane bending. International Journal of Fracture 70, 81–97.

Chen, M.C., Ping, X.C., 2007. Finite element analysis of piezoelectric corner configurations and cracks accounting for different electrical permeabilities. Engineering Fracture Mechanics 74, 1511–1542.

Chen, M.C., Sze, K.Y., 2001. A novel hybrid finite element analysis of bimaterial wedge problems. Engineering Fracture Mechanics 68, 1463–1476.

Fu, X.R., Long, Y.Q., 2003. Analysis of plane notch problems with analytical trial functions' method. Engineering Mechanics (in Chinese) 20 (4), 33–38. 73.

Gómez, F.J., Elices, M., 2003. A fracture criterion for sharp V-notched samples. International Journal of Fracture 123, 163–175.

Gross, B., Mendelson, A., 1972. Plane elastic analysis of V-notched plates. International Journal of Fracture Mechanics 8 (3), 267–276.

Gross, B., Srawley, J.E., Brown, W.F., 1964. Stress intensity factors for a singular edge-notch tension specimen by boundary collocation. NASA TN D-2395.

Henshel, R.D., Shaw, K.G., 1976. Crack tip finite elements are unnecessary. International Journal for Numerical Methods in Engineering 9, 495–507.

Hwu, C., Kuo, T.L., 2007. A unified definition for stress intensity factors of interface corners and cracks. International Journal of Solids and Structures 44, 6340–6359.

Ioka, S., Masuda, K., Kubo, S., 2007. Singular stress field near the edge of interface of bonded dissimilar materials with an interlayer. International Journal of Solids and Structures 44, 6232–6238.

Labossiere, P.E.W., Dunn, M.L., 1999. Stress intensities at interface corners in anisotropic bimaterials. Engineering Fracture Mechanics 62, 555–575.

Livieri, P., Lazzarin, P., 2005. Fatigue strength of steel and aluminium welded joints based on generalised stress intensity factors and local strain energy values. International Journal of Fracture 133, 247–278.

Matsumoto, T., Tanaka, M., Obara, R., 2000. Computation of stress intensity factors of interface cracks based on interaction energy release rates and BEM sensitivity analysis. Engineering Fracture Mechanics 65, 683–702.

Mohammed, I., Liechti, K.M., 2001. The effect of corner angles in bimaterial structures. International Journal of Solids and Structures 38, 4375–4394.

Niu, Zhongrong, 1993. Nonlinear bending of the shallow spherical shells with variable thickness under axisymmetrical loads. Applied Mathematics and Mechanics 14 (11), 1023–1031.

Pageau, S.S., Joseph, P.F., Biggers, S.B., 1995. Finite element analysis of anisotropic materials with singular inplane stress fields. International Journal of Solids and Structures 32, 571–591.

Ping, X.C., Chen, M.C., Xie, J.L., 2008. Singular stress analyses of V-notched anisotropic plates based on a novel finite element method. Engineering Fracture Mechanics 75, 3819–3838.

Reedy Jr., E.D., Guess, T.R., 1993. Comparison of butt tensile strength data with interface corner stress intensity factor prediction. International Journal of Solids and Structures 30, 2929–2936.

Rice, J.R., 1988. Elastic fracture mechanics concepts for interfacial cracks. ASME Journal of Applied Mechanics 55, 98–103.

Seweryn, A., Molski, K., 1996. Elastic stress singularities and corresponding generalized stress intensity factors for angular corners under various boundary conditions. Engineering Fracture Mechanics 55, 529–556.

Seweryn, A., 2002. Modeling of singular stress fields using finite element method. International Journal of Solids and Structures 39, 4787–4804.

Stern, M., Becker, E.B., Dunham, R.S., 1976. A contour integral computation of mixed-mode stress intensity factors. International Journal of Fracture 12 (3), 359–368.

Szabó, B.A., Yosibash, Z., 1996. Numerical analysis of singularities in two dimensions. Part 2: computation of generalized flux/stress intensity factors. International Journal for Numerical Methods in Engineering 39, 409–434.

Sze, K.Y., Wang, H.T., Fan, H., 2001. A finite element approach for computing edge singularities in piezoelectric materials. International Journal of Solids and Structures 38, 9233–9252.

Tan, C.L., Gao, Y.L., Afagh, F.F., 1992. Boundary element analysis of interface cracks between dissimilar anisotropic materials. International Journal of Solids and Structures 29, 3201–3220.

The Aeronautical Research Institute of China, 1993. Handbook of the Stress Intensity Factors. Science Press, Beijing (in Chinese).

Ting, T.C.T., 1996. Anisotropic Elasticity: Theory and Applications. Oxford University Press, London.

Williams, M.L., 1952. Stress singularities resulting from various boundary conditions is angular corners of plates in tension. Journal of Applied Mechanics 19, 526–528.

Xu, J.Q., Liu, Y.H., Wang, X.G., 1999. Numerical method for the determination of multiple stress singularities and related stress intensity coefficients. Engineering Fracture Mechanics 63, 775–790.

Yao, X.F., Yeh, H.Y., Xu, W., 2006. Fracture investigation at V-notch tip using coherent gradient sensing (CGS). International Journal of Solids and Structures 43, 1189–1200.

Yosibash, Z., Szabó, B.A., 1996. A note on numerically computed eigenfunctions and generalized stress intensity factors associated with singular points. Engineering Fracture Mechanics 54 (4), 593–595.